Journal of the Taiwan Institute of Chemical Engineers 132 (2022) 104132

Contents lists available at ScienceDirect

Journal of the Taiwan Institute of Chemical Engineers

journal homepage: www.elsevier.com/locate/jtice

A mixed matrix membrane for enhanced CO_2/N_2 separation via aligning hierarchical porous zeolite with a polyethersulfone based comb-like polymer

Yunfei Yu[a], Chenchen Zhang[a], Jiufeng Fan[b], Dongxia Liu[b,*], Jianqiang Meng[a,*]

[a] State Key Laboratory of Separation Membranes and Membrane Processes, School of materials science and Engineering, Tiangong University, Tianjin 300387, PR China

[b] Department of Chemical and Biomolecular Engineering, University of Maryland, College Park, MD,20742,USA

ARTICLE INFO

Article History:
Received 3 August 2021
Revised 25 October 2021
Accepted 28 October 2021
Available online 12 November 2021

Keywords:
Mixed matrix membranes
CO_2/N_2 separation
Pillared MFI zeolite nanosheets
Hierarchical porous
Comb-like copolymer

ABSTRACT

Background: Mixed matrix membranes (MMM)s for CO_2/N_2 separation still suffer from interfacial defects.
Method: To address this, a series of MMMs were prepared using polyethersulfone-g-poly (ethylene glycol) (PES-g-PEG) comb-like copolymer to tune the interfacial interaction with a pillared MFI (PMFI) zeolite nanosheets, which has a hierarchical porous structure to improve permeance. The composite membranes were examined by SEM, EDX and XRD. The dependence of gas permeabilities, diffusion and solubility coefficients of CO_2 and N_2 were determined by the time-lag method.
Results: The increase in PMFI zeolite loading led to an increase in the permeability coefficient of CO_2, which is mainly caused by the increase in CO_2 diffusion coefficient. The CO_2/N_2 gas separation was optimized at a loading of 20wt% PMFI zeolite, which produces a composite membrane with a CO_2 permeability of 66.9 Barrer and an ideal permeability selectivity coefficient of 9.6.

1. Introduction

The rising carbon dioxide (CO_2) concentration in the atmosphere has caused global climate change due to the serious greenhouse effect. Carbon dioxide enters the atmosphere mainly through the direct release of exhaust gases from combustions of fossil fuels, solid wastes and biomasses for energy production and from chemical processes such as cement manufacturing for materials/chemicals supplies for the society. Despite the negative impact of CO_2 on climate change, the wide demands for energy, materials and chemicals from the society drive the continuous operation of the combustion and manufacturing processes accompanied with continuous CO_2 production [1-4]. To avoid the entrance of CO_2 into atmosphere, the effluent streams from industrial processes could be processed by membrane separation followed by CO_2 sequestration. In addition, CO_2 existed in current atmosphere could be removed by the membrane separation. Therefore, the development of membrane materials for CO_2 separation and recycling processes has become an important task [5].

At present, the membranes for CO_2 separation are mainly made of inorganic, organic or mixed matrix materials. Inorganic membranes often have excellent thermal and chemical resistance, and high permeability coefficient, but suffer from high production cost and difficulty of up-scaling for industrial production. Organic membranes are mostly made of high-molecular polymers, which have abundant raw materials, low cost, easy processing and molding, and good mechanical properties [6]. The low permeability coefficient, however, limits its development. The mixed matrix membranes (MMMs) integrate organic and inorganic materials into one body which present performance advantages of both inorganic and organic membranes [7-9]. The combination of organic and inorganic phases in MMMs could produce a synergistic effect, in which rigid inorganic fillers provide excellent permeability for separation, while the flexible polymers make the feasibility of machinability and economicability [10]. Therefore, MMMs could remarkably surpass the solely polymeric or inorganic membranes.

In MMMs, the porous inorganic fillers that provide molecular transport highways require high loadings to achieve percolation. Currently MMMs, however, suffer from poor compatibility between the polymer matrix and the inorganic nanoparticles when the loading is high which causes interface defects [11-13]. The amphiphilic graft copolymer could tune the interfacial interaction between polymer matrix and the dispersed inorganic particles because the soft segment such as polyethylene glycol (PEG) has a good compatibility with the nanoparticle filler. Jong Hak Kim and coworkers have fabricated a series of amphiphilic graft copolymer MMMs for gas separation [14-16]. Amphiphilic comb-like polymers Poly(vinyl chloride)-g-

* Correspondence to: Jianqiang Meng, dongxia Liu
E-mail addresses: liud@umd.edu (D. Liu), jianqiang.meng@hotmail.com, jianqiang.meng@tiangong.edu.cn (J. Meng).

https://doi.org/10.1016/j.jtice.2021.10.032
1876-1070/

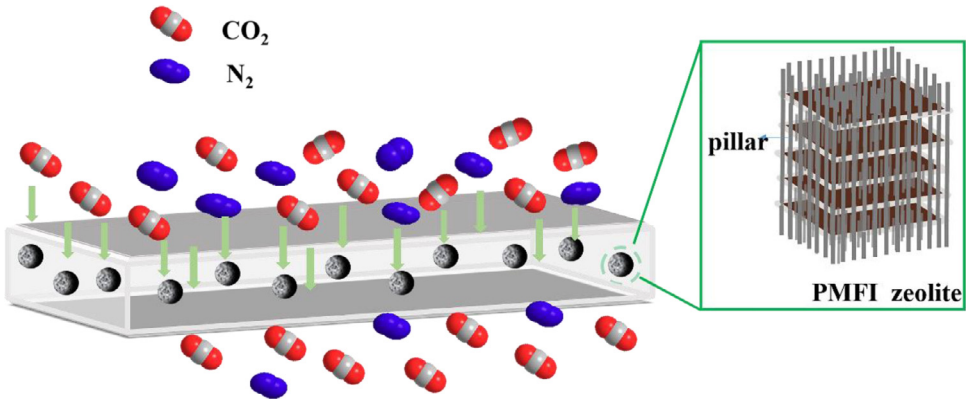

Fig. 1. The schematic diagram of MMM for CO_2/N_2 separation

poly(oxyethylene methacrylate)(PVC-g-POEM), poly(glycidyl methacrylate-co-poly(oxyethylene methacrylate)) (PGMA-co-POEM) and block copolymer poly (styrene-b-butadiene-b-styrene) (SBS) were used for dispersion of organic fillers, such as ZIF-8 or UiO-66, for CO_2 capture. The resulting MMMs show good permeation properties and uniform distribution of inorganic fillers, indicating the importance of amphiphilic graft copolymer in tuning the interface and interaction between the inorganic filler and the polymer matrix. The CO_2/N_2 separation performance of typical mixed matrix membranes based on comb or graft copolymer was summarized, as shown in Table S1.

Zeolite is an important inorganic filler to prepare the MMMs [17-19]. However, most zeolites used for MMMs preparation have three dimensional (3D) microporous structures that lack of molecular transport highways for high permeability of the resulting MMMs. For example, Ning Liu et al. [20] prepared a mixed matrix membrane with polyethersulfone as the polymer matrix and 3D MFI zeolite as the inorganic filler. MFI zeolite consists of two interconnected 10 membered ring (MR) pore systems: one is a straight channel running along the b-axis direction (5.3 × 5.6 Å); and the other is a zigzag channel running parallel to the a-axis (5.1 × 5.5 Å). Due to the lack of molecular transport channels, the permeability coefficient of MMM is only 10.6 Barrer at 35°C. In recent years, new synthesis techniques have given access to 2D zeolite nanosheets with small diffusion path lengths and accelerated molecular diffusion [21]. These 2D nanolayered materials include layered zeolites, porous graphenes, layered aluminophosphates and porous layered oxides [22]. Sankar Nair et al. [23] reported the molecular sieving membranes by coating MFI nanosheets on macroporous hollow fiber support. The membrane exhibited high performance for separation of n-butane from i-butane, and for other hydrocarbon separations. Sankar Nair et al. [24] also compared two kinds of sodium alginate (SA) matrix hybrid membranes loading with 2D-nanosheets and 0D-nanoparticles, respectively. The study demonstrated the superiority of the two-dimensional nanosheets over zero-dimensional nanoparticles as porous fillers, which could broaden the application of two-dimensional materials in membrane separation processes.

The advancement in zeolite synthesis has created diverse hierarchical 2D zeolite structures that incorporate meso- and even macropores for molecular transport. For example, the 2D pillared MFI (PMFI) zeolite nanosheets were reported by Ryoo's group [25]. In comparison to 3D MFI, the PMFI contains mesopores created by the SiO_2 pillars running between 2D zeolite nanosheet layers, parallel to the zigzag channels and perpendicular to the straight channel within the layers. The typical interlayer distance is ~4 nm and the shrinkage of zeolite thickness down to a few nanometers created abundant surface silanol (Si-OH) groups [26]. Therefore, PMFI zeolite bears the structural features of (i) the presence of mesopores facilitating molecular transport, (ii) the co-existence of multi-stage meso-/micropore structures shortening the molecular diffusion path, and (iii) sufficient surface Si-OH groups, which could be an ideal candidate for inorganic fillers in MMMs for enhancing CO_2/N_2 gas separations.

In our previous work, a comb-like copolymer polyethersulfone-g-polyethylene glycol (PES-g-PEG) was synthesized and its gas permeation and separation performance were studied [27]. As a results, the selectivity coefficient and the permeability coefficient of the PES A-g-PEG membrane increased with increasing PEG side chain density. The reason can be attributed to the fact that the higher PEG side chain density accompanies with the larger PEG micro phase dimension and more developed micro-phase separation. In these PEG micro regions, the quadrupole moment in CO_2 can interact well with the ethoxy polar groups in PEG. In continuation to our efforts in enabling effective CO_2 separation from CO_2 mixture gases, in this work, we prepared MMMs using PMFI zeolite nanosheets as inorganic fillers and the PES A-g-PEG copolymer as the membrane matrix. The hierarchical porous structure of PMFI zeolite is used as gas transport channel to improve the CO_2 permeability coefficient. The schematic diagram of MMM for CO_2 separation is shown as Figure 1. The morphological and textural properties of zeolite fillers was characterized by X-ray diffraction (XRD), scanning electron microscopy (SEM), and N_2 isotherm measurements. XRD and SEM observations were also used to characterize the influences of zeolite loadings on the crystallinity and surface morphology of the MMMs. A gas permeability instrument was used to test the gas permeability of the MMMs, and the dissolution and diffusion behavior of the gas in the membrane was analyzed theoretically based on the dissolution-diffusion theory. As far as we know, this is the first attempt that the PMFI zeolite nanosheets has been used as an inorganic filler to prepare a mixed matrix membrane for enhancing CO_2 permeability.

2. Experimental Section

2.1. Materials

Polyether sulfone grafted polyethylene glycol comb-like copolymer (PES-G-PEG550) was synthesized following the procedure reported from previous work [27]; N,N-dimethylformamide(DMF, 99.0 %) was purchased from Kermel (Tianjin, China); The PMFI zeolite was synthesized by pillaring of 2D multilamellar MFI zeolite. The synthesis of multilamellar MFI was done using the method reported by Ryoo and co-workers [25]. Pillaring of multilamellar MFI was done as reported by Na et al. to produce PMFI [26].

2.2. Preparation of the PES-g-PEG550/PMFI mixed matrix membrane

The membrane casting solution was firstly prepared by dissolving PES-g-PEG550 in DMF under stirring for 24 h, followed by adding a

Table 1
The components of PES A-g-PEG550/PMFI mixed matrix membrane

PMFI (wt%)	PES A-g-PEG550	PMFI	DMF
5wt%	0.238g	0.013g	4.75g
10wt%	0.225g	0.025g	4.75g
20wt%	0.200g	0.050g	4.75g
30wt%	0.175g	0.075g	4.75g
40wt%	0.150g	0.100g	4.75g

certain amount of PMFI zeolite. The resultant mixture was sonicated for 1 h to fully disperse the PMFI zeolite, and the membrane casting solution with 5wt% PES-g-PEG550 was prepared. Table 1 summarizes all the compositions used for synthesizing the MMMs. Afterwards, the casting solution was placed in a vacuum oven for degassing for 2h, and then transferred into a glass petri dish with a diameter of 5 cm. The Petri dish was held at 60°C in an electric oven for 24 h. Lastly, the MMM was dried at 120°C in a vacuum oven for 24 h. The thickness of the MMMs were 50-80 um.

2.3. Characterization

Both PMFI zeolite and MMMs were examined by the X-ray diffraction analysis device with a BRUKER D8 DISCOVER (Cu Kα radiation, λ=1.54 Å). The power of device is 60 kV × 80 mA and the scanning angle range was 5-45°. The morphology of MMMs was studied by field emission scanning electron microscopy (FE-SEM, ZEISS Gemini SEM50003040702). The FE-SEM used thermal field emission Schottky electron gun and the resolution can reach 0.6 nm@15 kV, 1.1 nm@1kV and 1.4 nm@500 V. Its acceleration voltage is 0.02-30kV, the electron beam current is 3 pA-20 nA, and the magnification is 12-2,000,000. Transmission electron microscope (TEM) images were taken with a Hitachi H7650 with an accelerating voltage of 120 kV (point resolution 0.204 nm). The EDX analysis of the MMMs used a thermal field characteristic X-ray energy spectrometer (EDAX OCTANE SUPER, USA). Its detection area is 60 mm*mm and the detection range of energy spectrum elements are Be4-U92. The specific surface area, pore size distribution and CO_2/N_2 adsorption selectivity analysis of PMFI zeolite were performed with a specific surface area and pore size micropore analyzer (3H-2000, BSD INSTRUMENT). The mechanical strength and properties of membranes were studied using the Precision electronic universal testing machine (AGS-X, SHIMADZU, Japan) with an operating head load of 50N. The testing speed was set at a rate of 10 mm/min and the test was repeated three times. In situ Fourier transform infrared spectroscopy (FTIR) was conducted with a Vertex80 Fourier transform infrared spectrometer from BRUKER (Germany). Its spectral range is 7500-370 cm^{-1}, the resolution is better than 0.07 cm^{-1} and the temperature range is 25-500°C. The test temperature was set to be 450°C so that the interference of water adsorption can be eliminated.

2.4. Gas permeation measurements

The constant volume method was used to test the pure gas permeability coefficient of the MMMs. The test temperature was 35°C and the test pressure was 1 atm. The unit of permeability coefficient (P) was Barrer (1 Barrer=10^{-10} cm^3 (STP) cm^{-1} s^{-1} cm Hg^{-1}).

When the pressure on the downstream side of the membrane changes steadily, the slope of the pressure-time curve can be used to calculate the gas permeability coefficient. As shown in Equation (1) [28].

$$P = \frac{273 \times 10^{10}}{760} \frac{VL}{AT(p_2 \times 76/14.7)} \left(\frac{dp}{dt}\right) \quad (1)$$

where P (Barrer) is the permeability coefficient of the gas, V (cm^3) is downstream gas storage tank volume of the membrane, L (cm) is the thickness of the membrane, A (cm^2) is the effective area of the test, T (K) is the test temperature, p_2 (psi) is the test pressure on the upstream side of the membrane, (dp/dt) referred to the slope of the pressure-time curve when the downstream side pressure changed steadily.

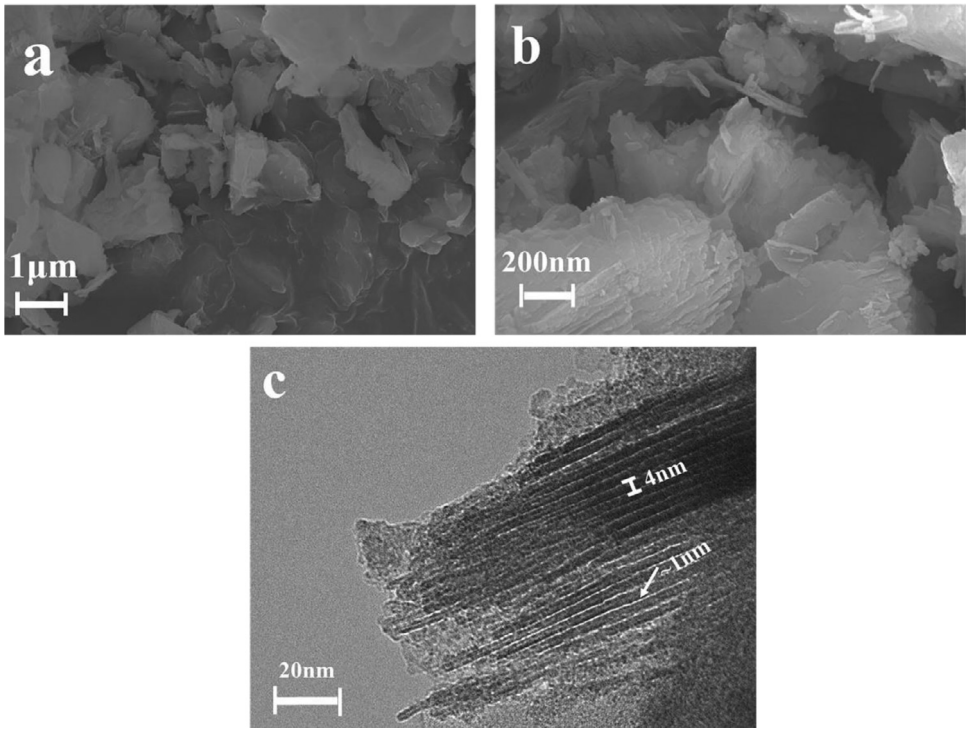

Fig. 2. SEM (a, b) and TEM (c) images of PMFI zeolite

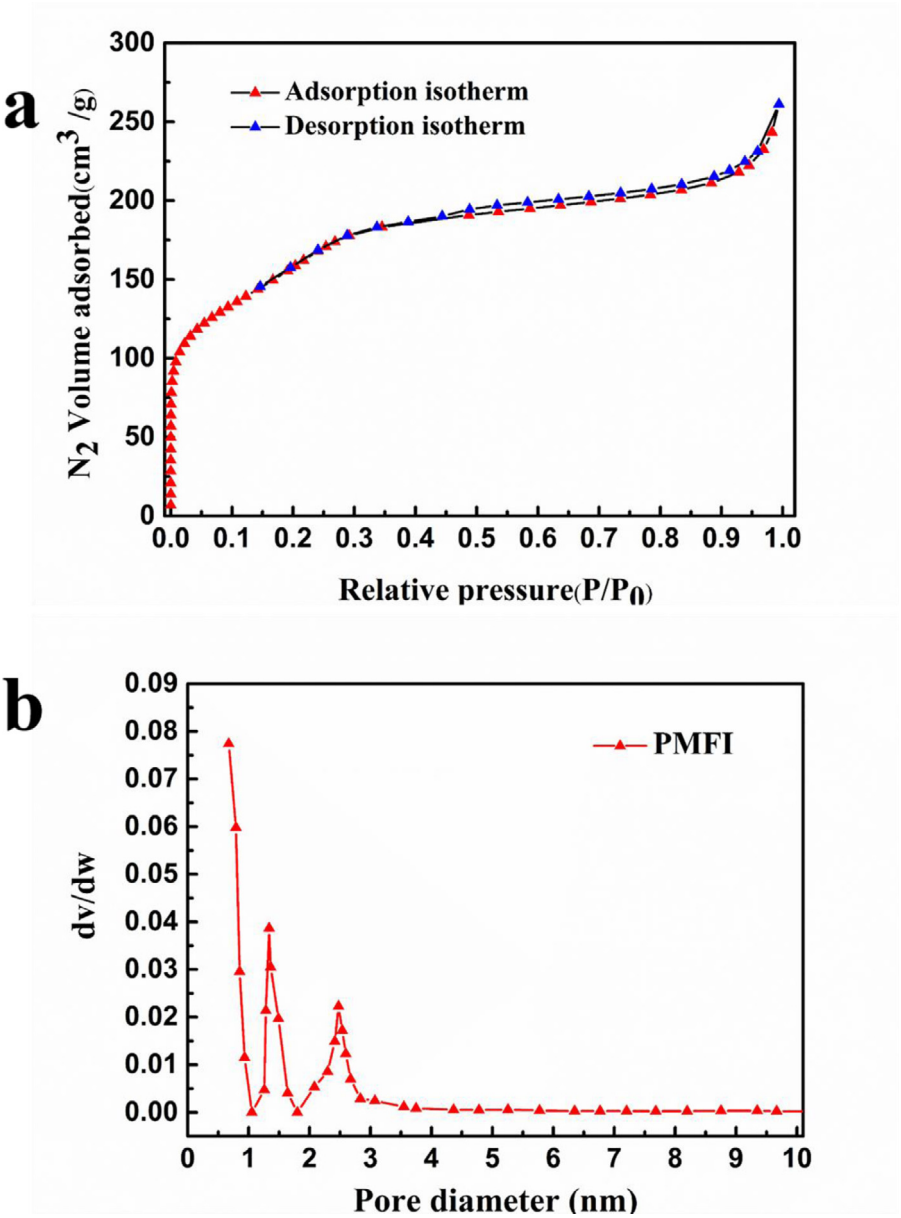

Fig. 3. PMFI zeolite (a) N_2 adsorption/desorption isotherms and (b) DFT pore size distribution (Before the test, vacuum degassing at 250°C for 12 h; N_2 adsorption-desorption test at 77 K)

Gas diffusivity coefficient was calculated by the time-lag method which is shown in Equation (2) [29]. The calculation of solubility coefficient is shown in Equation (3).

$$D = \frac{L}{6\theta} \tag{2}$$

$$S = \frac{P}{D} \tag{3}$$

where θ is the time-lag which is extrapolated from the measured downstream side pressure curve under steady state, and L (cm) is the thickness of the membrane.

As shown in Equation (4) [30], the ideal permeability selectivity coefficient is defined as the ratio of the permeability coefficient of gas i (easily permeates the membrane) to the permeability coefficient of gas j (difficult to permeate the membrane). It can also be expressed by the solubility coefficient and the diffusion coefficient.

$$\alpha_{ij} = \frac{P_i}{P_j} = \left(\frac{D_i}{D_j}\right) \times \left(\frac{S_i}{S_j}\right) \tag{4}$$

3. Results and Discussion

3.1. Characterization for PMFI zeolite

The morphology of PMFI zeolite was directly observed by a scanning electron microscope. As shown in Fig.2a, PMFI zeolite is composed of irregular shaped particles with a range of sizes. A closer look of the PMFI particles in Fig. 2b shows that the particles have plate- or flake-like morphology and some nanosheets peeled off from the particle surfaces. And the structure of PMFI zeolite was directly observed by a transmission electron microscope. It can be observed from Fig. 2c that several single-layer unit-thick zeolite nanosheets are arranged in parallel to each other and superimposed together to form a nano-zeolite assembly. There is a certain gap between the layers, which is caused by the presence of silica nanopillars between the nanosheets. The layer spacing is 4nm, and the thickness of the MFI sheet is 1nm.

The PMFI zeolite was further characterized by measuring its specific surface area, pore size distribution and adsorption selectivity. As shown in Fig.3a, the adsorption-desorption curve of PMFI zeolite

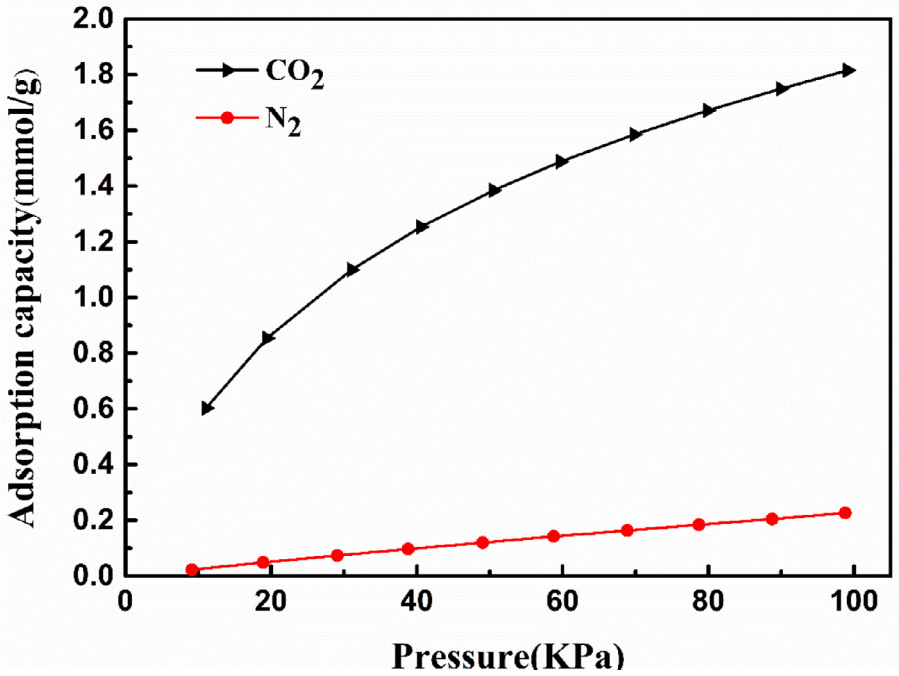

Fig. 4. Adsorption isotherms for CO_2 and N_2 on PMFI zeolite at 273 K. (Before the test, vacuum degassing at 250°C for 12 h)

belongs to the typelisotherm. When the relative pressure (P/P_0) was low, the adsorption characteristics of micropores were obvious. With increasing relative pressure P/P_0 from 0.15 to 0.90, the N_2 update by adsorption increases significantly which is caused by the mesopores in PMFI zeolite. Fig. 3b shows the pore sizes of PMFI zeolite are 1.5 nm and 2.5 nm. Among them, the pores of 1.5 nm were micropores on the zeolite layer of PMFI and the pores of 2.5 nm were mesopores between layers. The specific surface area of PMFI was 564.5 m^2/g and the pore volume was 0.41 cm^3/g, which are calculated by the Brunauer-Emmett-Teller (BET) multipoint method; the specific surface area of the micropores was 472.3 m^2/g and the volume of the micropores was 0.24 cm^3/g, which are calculated by the T-Plot method. Obviously, micropores account for a large proportion of specific surface area, and the hierarchical porous structure should be conducive to the adsorption and diffusion of gas molecules.

Fig.4 shows the adsorption isotherms of PMFI zeolite for CO_2 and N_2 at 273K. At 100 KPa, the adsorption capacity of PMFI zeolite for CO_2 was 1.8 mmol/g, and the adsorption capacity for N_2 was 0.22 mmol/g. The adsorption capacity of CO_2 was significantly higher than N_2, indicating that PMFI had a better affinity for CO_2, and the adsorption selectivity was 8.2. This is due to high concentration of silanol groups on the surface of PMFI zeolite, and the silanol groups have a good affinity with CO_2 and can freely interact with CO_2. As shown in Fig S1, the bands at 3745 cm^{-1} can be attributed to the stretching vibration bands of Si-OH bonds, which indicated the presence of large number of silanol groups on the surface of PFMI zeolite. At the same time, the CO_2-philic characteristics of the PMFI zeolite also contribute to improve the CO_2 permeability of MMM [31-33].

3.2. PMFI Mixed Matrix Membrane (MMM) characterization

The morphology of MMM plays an important role in determining its transport properties. In order to observe the influence of inorganic particle loading on the surface morphology and cross-sectional morphology of the MMM, a scanning electron microscope was used to characterize the MMM. As shown in Fig. 5, the membrane surface was dense, and PMFI zeolite particles were evenly distributed in the polymer matrix of the membrane. The interface between PMFI zeolite and PES A-g-PEG550 did not produce cracks and voids, indicating that the good compatibility between these two components in the MMMs. As the zeolite loading increases, the number of zeolite particles that can be observed on the membrane surface increases, but the membrane surface was still dense without defects. When the zeolite concentration is very high, agglomeration of zeolite particles occurred that reduced the zeolite dispersibility, as shown in Fig.5e and Fig.5f. Clearly, the morphology of the membrane is dependent on the distribution of PMFI zeolite. As shown in Fig.5g and Fig.5h, the PES-g-PEG comb-like polymer membrane showed a flat cross section, while the membrane with a PMFI zeolite content of 20wt% showed a rough cross section. And it becomes much more difficult to observe isolated PMFI zeolite and polymer matrix regions. The interconnectivity of PMFI zeolite will form interconnected network and provide pathway for gas transport in polymer. It can be seen that the PMFI zeolite particles in MMMs (20wt%, Fig.5d and Fig.5h) were well wrapped by the PES Ag-PEG550 matrix, and the zeolite particles were well combined with the matrix without obvious voids and cavities. In summary, when the zeolite loading in the mixed matrix membrane was less than 20wt%, the zeolite particles were uniformly distributed in the MMM.

In order to further explore the distribution of PMFI zeolite in MMM, X-ray energy spectrometer was used for analysis. Because PMFI zeolite contain silicon, it was selected as the measuring element, as shown by the red dot in Fig.6. It can be seen that as the PMFI zeolite content increased, the zeolite content on the membrane surface also gradually increased; and when the zeolite content was high, such as 30wt%, 40wt%, a large number of particles agglomerate together, resulting in clustered particle distribution. The agglomeration of zeolite particles may cause interparticle voids or defects between the zeolite and the polymer matrix interface, and affect the gas separation performance of the membrane. However, in order to increase the number of zeolite channels and increase the gas permeability coefficient, it is necessary to add as much zeolite as possible. When the amount of zeolite added is 20wt%, the amount of zeolite added is more appropriate.

To further confirm the effect of PMFI zeolite on the structure of MMMs, X-ray diffraction was carried out. It can be seen from Fig.7 that

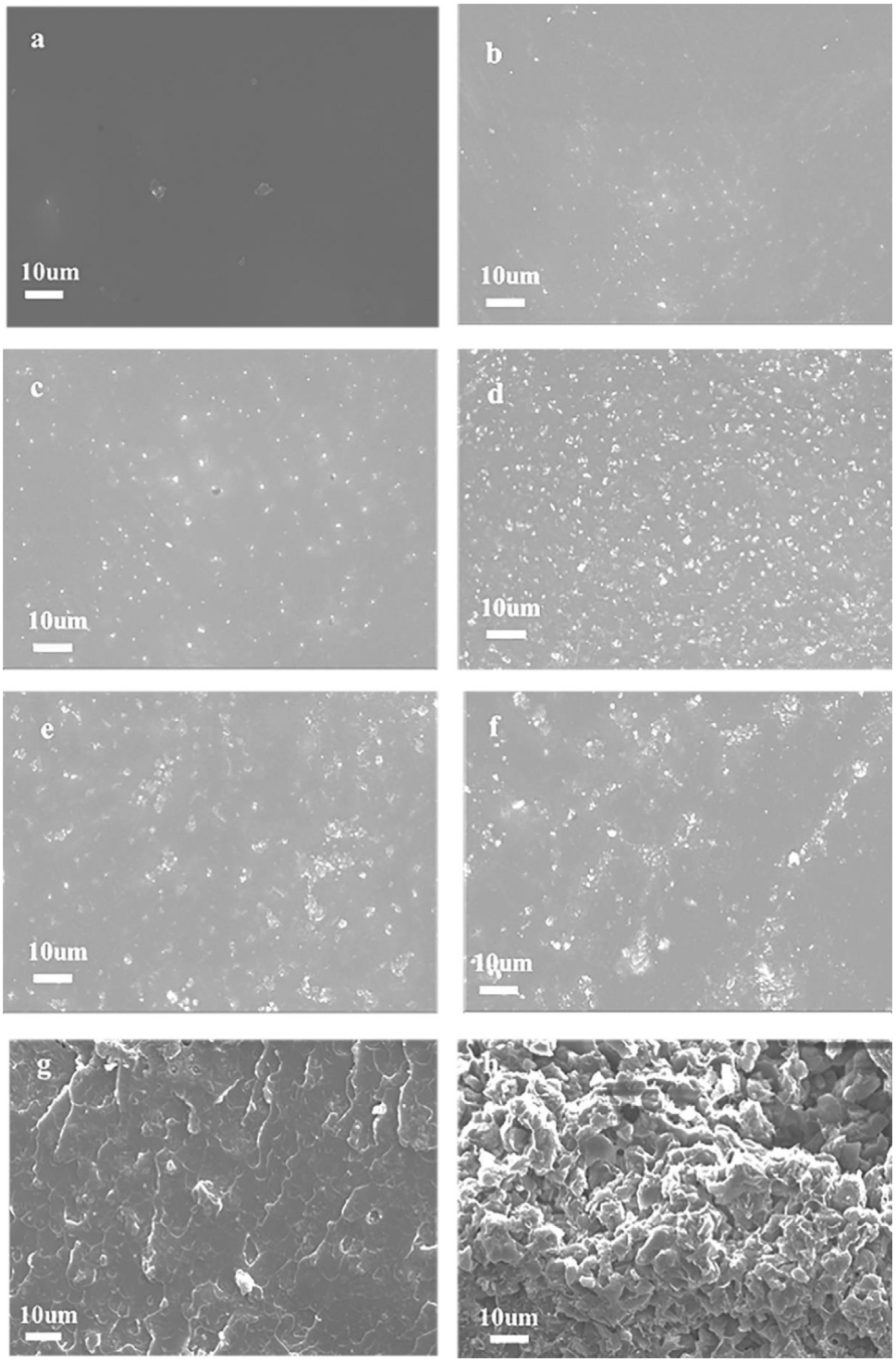

Fig. 5. SEM surface (a-f) and cross-section (g, h) images for mixed matrix membrane with different zeolite contents (a and g:0wt%; b:5wt%; c:10wt%; d and h:20wt%; e:30wt%; f:40wt%)

PMFI had a diffraction peak at 2θ=7.9°, 2θ=8.8°, 2θ=23.3°, 2θ=24.0°, which is consistent with the diffraction peak position of standard PMFI. After adding PFMI zeolite particles, MMMs showed diffraction peaks at 2θ=7.9°, 2θ=8.8°, 2θ=23.3°, 2θ=24.0°, and the more the added amount, the stronger the diffraction peaks. Meanwhile, the wide dispersion peak of MMMs at 2θ=20° did not disappear, indicating that the amorphous morphology of the polymer matrix did not disappear even after the addition of highly crystalline PFMI particles. However, with the increase in PMFI zeolite contents in the MMMs, the d-spacing gradually decreased because the addition of inorganic fillers restricted the polymer chain mobility. And the peak intensity also gradually decreased with the PMFI zeolite contents increase at 2θ=20°. The decrease in peak intensity indicates that part of orderly packed polymeric structure is destroyed due to which the intensity of the characteristic peak is reduced [34-36].

The tensile strength and elongation at break of mixed matrix membranes were summarized in Fig. 8. The tensile strength of mixed matrix membranes decreased after adding PMFI zeolites but still higher than other reported graft copolymer mixed matrix

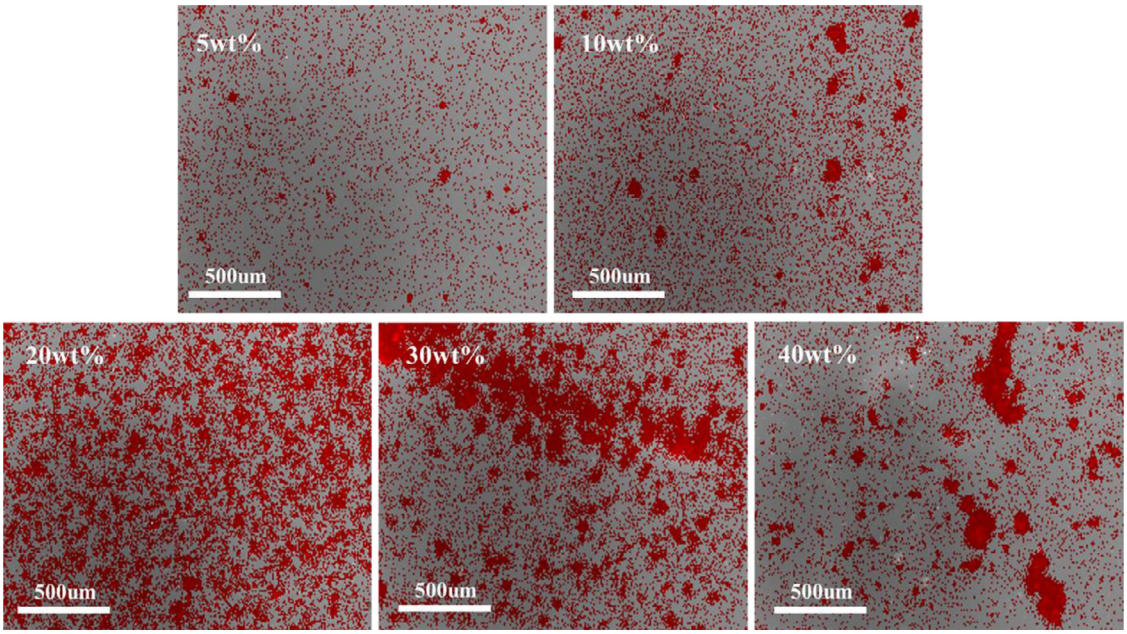

Fig. 6. EDX analysis of mixed matrix membrane with different loading (%) of the PMFI nanosheets

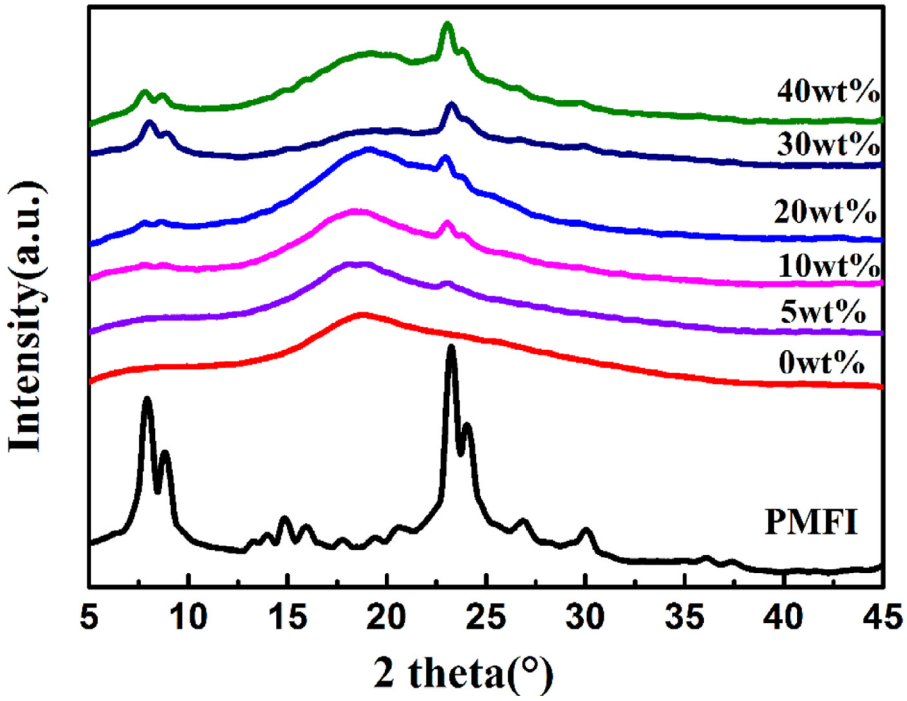

Fig. 7. XRD patterns of mixed matrix membranes and PMFI zeolite

membranes [16]. The mechanical strength of the MMM was mainly provided by the rigid hydrophobic PES blocks, while partial PMFI zeolites fillers disrupt the structure of the matrix. This is mainly due to mismatch between the rigid inorganic filler and the rigid organic matrix. The PMFI zeolites fillers would be mainly wrapped by the soft PEG blocks due to a lack of strong interactions between the rigid PES blocks and the fillers. Therefore, the tensile strength and the elongation at break of mixed matrix membranes decreased upon PMFI [37].

3.3. *Performance of mixed matrix membrane on gas permeation*

The permeability of the MMMs to pure CO_2 and N_2 was measured with the constant volume method. The test temperature is 35°C and the pressure is 1 atm. The results were shown in Fig.9 and Table S2. It can be seen that with the increase in PMFI zeolite loading, the permeability coefficient of CO_2 showed an upward trend. According to pore size distribution of PMFI zeolite, the mesopore diameters are 1.5 nm and 2.5 nm, which are much larger than the dynamic diameter of gas molecules (CO_2: 0.33 nm, N_2: 0.36 nm). After the PMFI zeolite particles were added, gas molecules could easily pass through the pore channels in the PMFI zeolite to reduce the transport resistance. On the other hand, the strong interaction between polymer chains segment and PMFI zeolite nanosheets may disrupt the polymer chain packing and increase the void and thus enhance the gas diffusion [7,10]. The XRD results also prove this fact. It is noted in Table.2 that when the amount of zeolite was 5wt%, the diffusion

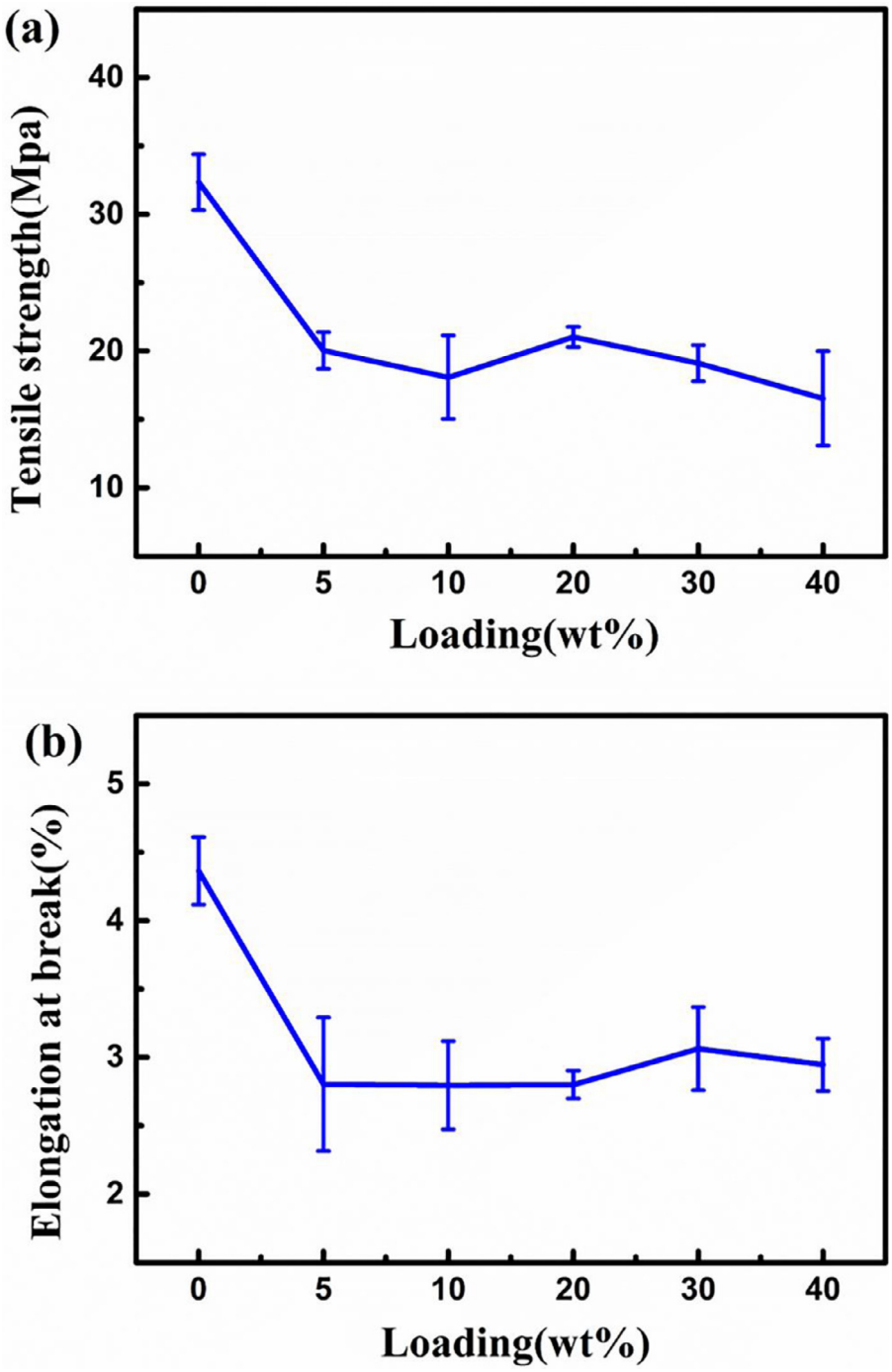

Fig. 8. Tensile strength (a) and elongation at break (b) of mixed matrix membranes with different loading.

coefficient of CO_2 was 10 times higher than that without adding zeolite; and when the amount of zeolite was 40wt%, the diffusion coefficient of CO_2 was increased by 20 times. Therefore, the increase in CO_2 permeability coefficient was mainly due to the increase in CO_2 diffusion coefficient. However, ideal permeability selectivity coefficient of MMMs are reduced after the initial addition of zeolite because the PMFI zeolite nanosheets have no molecular sieving effect.

When the zeolite loading was higher (i.e., 30wt%, 40wt%), the ideal permeability selectivity coefficient decreases. For example, the MMM with a PMFI zeolite loading of 40wt% has 423.0 Barrer permeability, which was 32-fold enhancement compared to the MMM made of bare PES A-g-PEG550 polymer. However, the ideal permeability selectivity coefficient for CO_2/N_2 was severely reduced to 1.15. This should be caused by the particle agglomeration, as confirmed by the EDX and SEM analyses. The large particles do not have strong interfacial interaction with the polymer matrix which might form the interfacial voids. At this condition, the Knudsen diffusion of gas molecules was dominant, so the permeability coefficient of N_2 increased and the ideal permeability selectivity coefficient decreased. In addition, the mesopore in the PMFI zeolite has no molecular sieving effect, which should provide a convective channel and is also the reason for the reduction of the ideal permeability selectivity coefficient.

When the zeolite loading is low (5wt%, 10wt%, 20wt%), the CO_2 permeability coefficient and the ideal permeability selectivity

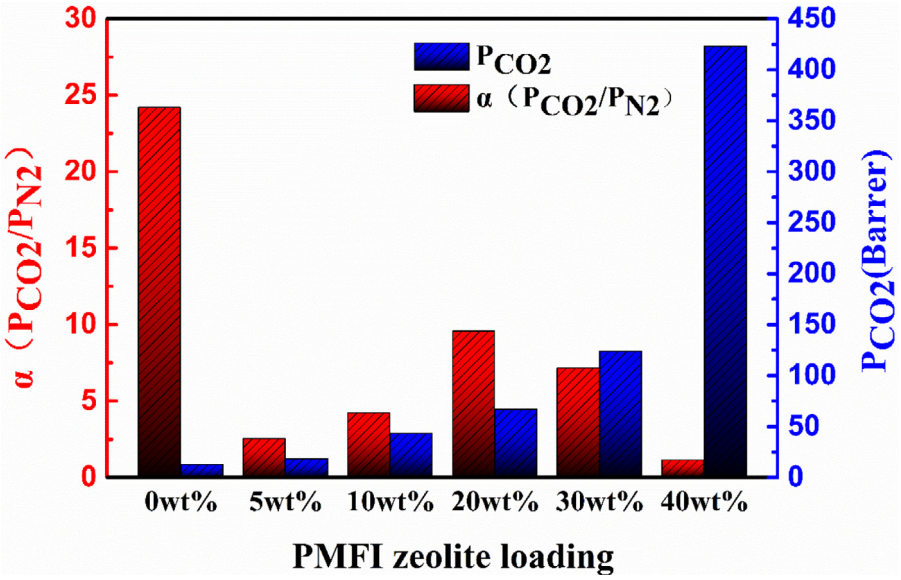

Fig. 9. PCO2 and $\alpha(P_{CO2}/P_{N2})$ of PES A-g-PEG550/PMFI mixed matrix membrane at 35°C and 1 atm.

coefficient simultaneously increased with the increase of PMFI zeolite loading. These improvements are obtained through an interface and interaction tuning approach based on an amphiphilic grafted copolymer. In addition, it also can be attributed to the high sorption selectivity of PMFI zeolite for CO_2 over N_2. With the increase of PMFI zeolite, the permeability coefficients of CO_2 and N_2 will increase but the permeability coefficient of CO_2 increases faster. Therefore, the ideal permeability selectivity coefficient increases according to Equation (4). When the PMFI zeolite loading is 20wt%, the gas separation performance of MMM is the best (P: 66.9 Barrer, α:9.6).

4. Conclusion

The mixed-matrix membranes were successfully fabricated by introducing the PMFI zeolite that has dual micro- and mesoporosity into the PES-g-PEG comb-like copolymer matrix. The effect of PMFI loading as the fillers on gas transport performance of the resultant MMMs were studied. The PMFI zeolite nanosheets shows good sorption selectivity of CO_2 to N_2 (8.2). Observed by SEM, the surface of the mixed matrix membrane is dense and has no obvious defects under lower PMFI zeolite loading (5wt%, 10wt%, 20wt%), PMFI zeolite nanosheets are uniformly dispersed in the polymer matrix; while under higher PMFI zeolite loading (30wt%, 40wt%), the zeolite particles agglomerated seriously, and the ideal permeability selectivity coefficient of the gas is reduced. When the PMFI zeolite loading is 20wt%, the obtained MMM shows the best CO_2 separation performance: the CO_2 permeability coefficient is 66.9 Barrer, which is 4 times higher than the original membrane; the ideal permeability selectivity coefficient is 9.6, which is about half of that of the original membrane.

Declaration of Competing Interest

The authors declare that they have no known competing financial interests or personal relationships that could have appeared to influence the work reported in this paper.

Acknowledgements

We gratefully acknowledge the support from the National Natural Science Foundation of China (Grant No. 21875162, 22075206)

Supplementary materials

Supplementary material associated with this article can be found, in the online version, at doi:10.1016/j.jtice.2021.10.032.

References

[1] Li Q, Liu S, Peng W, et al. Preparation of biomass-derived porous carbons by a facile method and application to CO2 adsorption[J]. Journal of the Taiwan Institute of Chemical Engineers 2020;116:128–36.
[2] Wang L, Yi Y, Guo H, et al. Atmospheric pressure and room temperature synthesis of methanol through plasma-catalytic hydrogenation of CO2[J]. Acs Catalysis; 2017.
[3] Bhatti U H, Sivanesan D, Lim D H, et al. Metal oxide catalyst-aided solvent regeneration: A promising method to economize post-combustion CO2 capture process[J]. Journal of the Taiwan Institute of Chemical Engineers 2018;93:150–7.
[4] Aresta M, Dibenedetto A, Angelini A. Catalysis for the Valorization of Exhaust Carbon: from CO2 to Chemicals, Materials, and Fuels. Technological Use of CO2 [J]. Chemical Reviews 2014;114(3):1709–42.
[5] Pan R H, Chen Y R, Tung K L, et al. Experimental and simulation study of a novel hybrid absorption and stripping membrane contactor for carbon capture[J]. Journal of the Taiwan Institute of Chemical Engineers 2017;81:47–56.
[6] Xing R, Ho WSW. Synthesis and characterization of crosslinked polyvinylalcohol/polyethyleneglycol blend membranes for CO2/CH4 separation[J]. Journal of the Taiwan Institute of Chemical Engineers 2009;40(6):654–62.
[7] Sarfraz M, Ba-Shammakh M. A novel zeolitic imidazolate framework based mixed-matrix membrane for efficient CO2 separation under wet conditions[J]. Journal of the Taiwan Institute of Chemical Engineers 2016;65:427–36.
[8] Koolivand H, Sharif A, Kashani M R, et al. Functionalized graphene oxide/polyimide nanocomposites as highly/CO2 selective membranes[J]. Journal of Polymer Research 2014;21(11):599.
[9] Sanaeepur H, Kargari A, Nasernejad B, et al. A novel Co2+ exchanged zeolite Y/cellulose acetate mixed matrix membrane for CO2/N2 separation[J]. Journal of the Taiwan Institute of Chemical Engineers 2016;60:403–13.
[10] Chen W, Zhang Z, Yang C, et al. PIM-based mixed-matrix membranes containing MOF-801/ionic liquid nanocomposites for enhanced CO2 separation performance [J]. Journal of Membrane Science 2021;636:119581.
[11] Su N C, Sun D T, Beavers C M, et al. Enhanced permeation arising from dual transport pathways in hybrid polymer–MOF membranes[J]. Energy & Environmental Science 2016;9(3):922–31.
[12] Guo X, Qiao Z, Liu D, et al. Mixed-matrix membranes for CO2 separation: role of the third component[J]. Journal of Materials Chemistry A 2019;7(43):24738–59.
[13] McKeown N B. A perfect match[J]. Nature materials 2018;17(3):216–7.
[14] Kim N U, Park B J, Lee J H, et al. High-performance ultrathin mixed-matrix membranes based on an adhesive PGMA-co-POEM comb-like copolymer for CO2 capture[J]. Journal of Materials Chemistry A 2019;7(24):14723–31.
[15] Chi W S, Kim S J, Lee S J, et al. Enhanced performance of mixed-matrix membranes through a graft copolymer-directed interface and interaction tuning approach [J]. ChemSusChem 2015;8(4):650–8.
[16] Kang D A, Kim K, Lim J Y, et al. Mixed matrix membranes consisting of ZIF-8 in rubbery amphiphilic copolymer: Simultaneous improvement in permeability and selectivity [J]. Chemical Engineering Research and Design 2020;153:175–86.

[17] Liu M, Gurr P A, Fu Q, et al. Two-dimensional nanosheet-based gas separation membranes [J]. Journal of Materials Chemistry A 2018;6(46):23169–96.
[18] Vinoba M, Bhagiyalakshmi M, Alqaheem Y, et al. Recent progress of fillers in mixed matrix membranes for CO2 separation: A review[J]. Separation and Purification Technology 2017;188:431–50.
[19] Dunn C A, Shi Z, Zhou R, et al. Cross-linked poly (ionic liquid)−ionic liquid−zeolite) mixed-matrix membranes for CO2/CH4 gas separations based on curable ionic liquid prepolymers[J]. Industrial & Engineering Chemistry Research, 2019;58(11):4704–8.
[20] Yu J, Li L, Liu N, et al. An approach to prepare defect-free PES/MFI-type zeolite mixed matrix membranes for CO2/N2 separation [J]. Journal of Materials Science 2013;48(10):3782–8.
[21] Knio O, Medford A J, Nair S, et al. Database of Computation-Ready 2D Zeolitic Slabs[J]. Chemistry of Materials 2018;31(2):353–64.
[22] Kim W, Nair S. Membranes from nanoporous 1D and 2D materials: A review of opportunities, developments, and challenges[J]. Chemical Engineering Science 2013;104:908–24.
[23] Min B, Yang S, Korde A, et al. Continuous zeolite MFI membranes fabricated from 2D MFI nanosheets on ceramic hollow fibers[J]. Angewandte Chemie International Edition 2019;58(24):8201–5.
[24] Liu G, Jiang Z, Cao K, et al. Pervaporation performance comparison of hybrid membranes filled with two-dimensional ZIF-L nanosheets and zero-dimensional ZIF-8 nanoparticles[J]. Journal of Membrane Science 2017;523:185–96.
[25] Choi M, Na K, Kim J, et al. Stable single-unit-cell nanosheets of zeolite MFI as active and long-lived catalysts[J]. Nature 2009;461(7261):246–9.
[26] Na K, Choi M, Park W, et al. Pillared MFI zeolite nanosheets of a single-unit-cell thickness[J]. Journal of the American Chemical Society 2010;132(12):4169–77.
[27] Yu Yunfei, et al. Tuning the micro-phase separation of the PES-g-PEG comb-like copolymer membrane for efficient CO2 separation. Separation and Purification Technology 2021:118465.
[28] Yang T, Chung T-S. High performance ZIF-8/PBI nano-composite membranes for high temperature hydrogen separation consisting of carbon monoxide and water vapor. International Journal of Hydrogen Energy 2013;38:229–39.
[29] Xu Z-K, Dannenberg C, Springer J, Banerjee S, Maier G. Novel poly(arylene ether) as membranes for gas separation. Journal of Membrane Science 2002;205:23–31.
[30] Senthilkumar U, Reddy BSR. Polysiloxanes with pendent bulky groups having amino-hydroxy functionality: Structure−permeability correlation. Journal of Membrane Science 2007;292:72–9.
[31] Kassaee M H, Sholl D S, Nair S. Preparation and gas adsorption characteristics of zeolite MFI crystals with organic-functionalized interiors[J]. The Journal of Physical Chemistry C 2011;115(40):19640–6.
[32] Witoon T, Tatan N, Rattanavichian P, et al. Preparation of silica xerogel with high silanol content from sodium silicate and its application as CO2 adsorbent[J]. Ceramics International 2011;37(7):2297–303.
[33] Ahmad M Z, Navarro M, Lhotka M, et al. Enhanced gas separation performance of 6FDA-DAM based mixed matrix membranes by incorporating MOF UiO-66 and its derivatives[J]. Journal of membrane science 2018;558:64–77.
[34] Sadeghi M, Khanbabaei G, Dehaghani A H S, et al. Gas permeation properties of ethylene vinyl acetate−silica nanocomposite membranes[J]. Journal of Membrane Science 2008;322(2):423–8.
[35] Xie J, Duan R G, Han Y, et al. Morphological, rheological and electrochemical studies of poly (ethylene oxide) electrolytes containing fumed silica nanoparticles[J]. Solid State Ionics 2004;175(1-4):755–8.
[36] Joly C, Goizet S, Schrotter J C, et al. Sol-gel polyimide-silica composite membrane: gas transport properties[J]. Journal of Membrane Science 1997;130(1-2):63–74.
[37] Li H, Tuo L, Yang K, et al. Simultaneous enhancement of mechanical properties and CO2 selectivity of ZIF-8 mixed matrix membranes: Interfacial toughening effect of ionic liquid[J]. Journal of Membrane Science 2016;511:130–42.